Journal of Electron Microscopy **48(6)**: 673–679 (1999)

Review

HAFN Special Issue

Localized valence spectroscopy of complex nanostructures

A. Howie[1,*], J. Aizpurua[2], F. J. Garcia de Abajo[3], and B. K. Rafferty[1]

[1]Cavendish Laboratory, University of Cambridge, Madingley Road, Cambridge CB3 0HE, UK, [2]Facultad de Quimicas, and [3]Facultad de Informatica, Universidad del Pais Vasco, E-20080 San Sebastian, Spain
*To whom correspondence should be addressed. E-mail: ah30@phy.cam.ac.uk

Abstract STEM valence loss spectra have an energy resolution of about 0.2 eV and a spatial resolution of about 1 nm. With developments of inhomogeneous dielectric excitation theory, detailed spectral interpretation is now becoming possible in the complex geometry of typical nanostructures. A non-relativistic, numerical approach based on the boundary charge method is outlined. This method gives useful results in good agreement with experiment for 90° wedges and truncated slabs. It appears that these results form a convenient basis for the interpretation of loss spectra from more complex shapes such as the T or I junctions arising when two dielectrics form an interface in a thin film. The numerical boundary method can be extended to the relativistic case to include retardation and radiation. Such computations of the radiation emitted by excited nanostructures are potentially useful for optical emission spectroscopy in the STM and NSOM as well as in the STEM.

Keywords EELS, valence excitation, inhomogeneous dielectric, boundary charge method, emitted radiation

Received 11 December 1998, accepted 23 February 1999

Introduction

Various forms of electron microscopy (TEM, SEM, STM) now have an established role in determination of geometrical structure on a nanometer scale. The power of this approach is greatly augmented when combined with some form of spatially localized spectroscopy to yield information about local composition or even about electronic structure. Core loss spectroscopy in the scanning transmission electron microscope (STEM) can be achieved with 0.2 nm spatial resolution and 0.2 eV energy resolution to provide information about local chemistry as well as the density of unoccupied electronic states. More direct information about occupied states is in principle available at better than 1 nm spatial resolution from the relatively more intense valence loss spectra which can usually be collected more rapidly with less risk of radiation damage. Further attractions of these lower energy excitations are their reasonable accessibility in the STM or near field SOM and the additional detection channel they provide of optical emission with potentially much higher energy resolution.

Although spatially localized valence loss spectroscopy has a long history in electron microscopy, its widespread use has been hampered by problems in interpreting the results. The loss spectra depend not only on the dielectric response of the different regions present but also on the geometry of the boundaries between them. Over the past two decades however these difficulties have been substantially overcome. The dielectric excitation problem can be solved analytically in the case of simple shapes such as planar [1–3], cylindrical [4,5] or spherical [6–10] interfaces and yields results in reasonably good agreement with the experimental observations. Study of these simple situations has also served to reveal the general structure of the theory for more complex geometries where numerical methods have to be employed.

At an impact parameter $\mathbf{b}$, the probability $P(\mathbf{b},\omega)$ for a given energy loss ω in a composite medium composed of two materials A and B depends in general on a linear combination of dielectric excitation functions. Each of these functions corresponds to an eigenmode j of the system and depends on the geometry. The frequency of the eigenmode is determined by the vanishing of the denominator in the excitation function.

$$P(\mathbf{b}, \omega) = \Sigma_j A_j (\omega b/v) \text{ Im } \{ -1/[\alpha_j \varepsilon_A + (1 - \alpha_j) \varepsilon_B] \} \quad (1)$$

The bulk losses in the two media A and B are described by the above excitation functions with $\alpha_j = 1$ and 0 respectively and far from any interface only the appropriate one of these functions appears in eq. (1). As a planar interface is approached, this bulk loss term is progressively replaced by a planar interface loss term characterized by $\alpha_j = 0.5$, the quantity $\Sigma_j A_j (\omega b/v)$ remaining constant (the so-called *Begrenzungs* effect). The familiar surface plasmon is a particular example arising at the free surface of material A say, when B is vacuum i.e. $\varepsilon_B = 1$. A particularly important planar interface mode is observed at about 8 eV in the case of the Si-SiO_2 boundary [11]. The simplest example of a non-planar boundary is provided by a small sphere of material A embedded in material B where the appropriate dipole mode excitation function has the value $\alpha_j = 1/3$. For a given geometry (which determines the quantities α_j and $A_j(\omega b/v)$), eq. (1) defines the loss spectrum for any choice of dielectric materials if the appropriate dielectric functions are used. Eq. (1) and the above sum rule both appear to be followed in much less simple situations, including for instance colloidal dispersions of small interacting particles [12,13] where an effective medium approach is appropriate.

In better defined but still complex geometries, eq. (1) provides an excellent basis for (non-relativistic) analysis of the localized loss spectra but numerical methods are needed to find the various eigenmodes (defined by a value of α_j) and the corresponding weight A_j with which they contribute to the loss spectrum at each impact parameter. In the following three sections, we outline the boundary charge method for solving such problems and some of the results obtained for structures often studied in transmission electron microscopy. We then briefly discuss the recently developed extension of this approach to the relativistic regime where retardation and radiative losses are included. Finally we make some concluding observations about the likely future usefulness of spatially resolved valence loss spectroscopy in various contexts of nanostructure characterization.

The boundary charge method

The method (originally used for electrostatic problems by Maxwell) depends on finding a self-consistent distribution of boundary charges on all the dielectric interfaces and was employed by Fuchs [14] to find the eigenmodes of a small cube and later reformulated by Ouyang and Isaacson [15,16] for energy loss problems. Aizpurua *et al.* [17–19] have applied the method to 90° wedges and other geometries such as a torus and coupled cylinders. We employ their notation to describe the self-consistent condition for the interface charge density $\sigma(\mathbf{s},\omega)$ in the presence of an external potential $\phi^{ext}(\mathbf{s},\omega)$ with frequency generated at an interface point $\mathbf{s}$ by a passing fast electron.

$$\Lambda(\omega)\sigma(\mathbf{s},\omega) = \frac{1}{4\pi\varepsilon_0 \mathbf{n}_s.\nabla\phi^{ext}(\mathbf{s},\omega) + \int d^2\mathbf{s}'\sigma(\mathbf{s}',\omega)\mathbf{n}_s.\nabla\frac{1}{|\mathbf{s}-\mathbf{s}'|}} \quad (2)$$

where

$$\Lambda(\omega) = 2\pi \frac{\varepsilon_B(\omega) + \varepsilon_A(\omega)}{\varepsilon_B(\omega) - \varepsilon_A(\omega)} \quad (3)$$

Here $\mathbf{n}_s$ is a unit vector at the point s on the interface directed normal to the interface from medium A to medium B. In the absence of the external potential, eq. (2) gives the eigenmodes $\sigma^j(\mathbf{s})$ and eigenvalues $2\pi\lambda_j$ of the system. With standard computer packages and an adequate number of sampling points (typically about 100) on the interface, the eigenmodes can readily be computed and, in the case of simple shapes like a sphere, checked against the known results. For any combination of the two dielectric materials, eq. (3) can then be employed, setting equal to each $2\pi\lambda_j$ value in turn to determine the mode frequencies which will in general be complex because of damping. It may be observed that interface charge interactions in a plane do not produce any electric field component normal to the plane so that all the eigenvalues $2\pi\lambda_j$ are zero in that case. Although the integrand in eq. (2) is not symetrical under interchange of $\mathbf{s}$ and $\mathbf{s}'$, the eigenvalues $2\pi\lambda_j$ can in general be shown to be real [15] and furthermore the eigenfunctions $\sigma^j(\mathbf{s})$ form a complete basis set, satisfying an orthogonality property.

$$\int d^2\mathbf{s}\int d^2\mathbf{s}' \frac{\sigma^i(\mathbf{s})\sigma^j(\mathbf{s}')^*}{|\mathbf{s}-\mathbf{s}'|} = \delta_{ij} \quad (4)$$

With the aid of this equation, the complete solution of eq. (2) can be obtained. The mode excitation functions appearing in eq. (1) then have $\alpha_j = (1 + \lambda_j)/2$.

For any particular interface charge distribution $\sigma(\mathbf{s},\omega)$, the stopping power and energy loss probability function $P(\mathbf{b},\omega)$ can be directly expressed by evaluating the electric field component E which it generates at the position of the fast electron. In determining the contribution A_j from each mode in eq. (1), the impact parameter in fact contributes twice— once in fixing the mode excitation and a second time in evaluating the field generated by that mode at the trajectory position. It is important to note that when only two dielectric media are involved the eigenmode computation need only be done once for each geometry and does not have to be redone if the dielectric functions are changed.

With the aid of standard computer packages, the theory just described can be employed to compute non-relativistic energy loss spectra near dielectric interfaces with a complex geometry. It is particularly efficient for interface shapes with axial symmetry or for cases, such as a dielectric wedge, which are independent of one coordinate z since all the quantities can then be expressed in terms of Fourier components q in this direction [17]. In such cases the interface charge density can often be adequately sampled

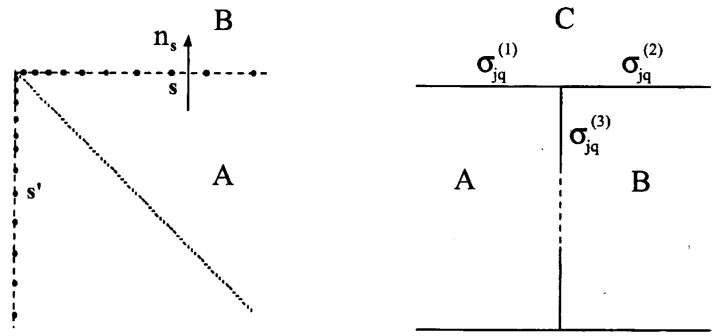

1(a) 1(b)

Fig. 1 Boundary charge arrangements for (a) an isolated 90° wedge and (b) the T junction components of the I junction in a thin film.

with as few as twenty points s. In more general situations, a few hundred points could be required. When the fast electron beam also travels parallel to the z direction, the situation becomes even simpler since by conservation of momentum only a single Fourier component $q = \omega/v$ is involved. For perpendicular or other more general trajectories, an integration over the contribution of modes of different q has to be carried out. The range of q values required is approximately defined by $|q_{max}| = 1/|b|$ where b is the impact parameter (or closest distance from the dielectric interface to the electron trajectory).

Energy loss spectra from wedges and truncated slabs

The 90° dielectric wedge in vacuum, whose eigenmodes have already been studied by a number of authors [20,21], provides an interesting and experimentally relevant illustration of the boundary charge method. Complications from the singularity at the wedge apex (where the surface normal is not defined) are minimized by taking surface points s as shown in Fig. 1a and examining the numerical results for convergence in terms of the number and spacing of points taken and in particular the distance d of the closest points from the wedge apex. Although mode frequencies are somewhat changed and extra modes appear if more points are inserted closer to the apex, these changes do not appreciably affect energy loss spectra of fast electrons provided $d < \beta v/\omega$ where $\beta = 0.1$. Because of the reflection symmetry of the wedge about the dotted diagonal in Fig. 1a, the modes can be classified as symmetrical or antisymmetrical for the surface charge distributions on the two limbs. If we denote these two charge distributions by $\sigma_{iq}{}^{(1)}(s)$ and $\sigma_{iq}{}^{(2)}(s)$ for a particular mode (now labelled by its wavevector q along the axis and a radial index j) we can rewrite the eigenvalue equation in a contracted form.

$$\Lambda(\omega)\sigma_{jq}{}^{(1)}(s) = -G_{jq}\,\sigma_{jq}{}^{(2)}(s);\ \Lambda(\omega)\sigma_{jq}{}^{(2)}(s) = -G_{jq}\,\sigma_{jq}{}^{(1)}(s) \quad (5)$$

Here the interaction integral G_{jq} is the same in both cases because of the reflection symmetry already noted and the planar structure of each limb ensures no self-interaction of the charge on each limb. For each set of indices j,q a symmetric and an antisymmetric mode arise with frequencies defined by $\Lambda(\omega) = -G_{jq}$ and $\Lambda(\omega) = G_{jq}$ respectively. Referring to equations (1) and (3), we then see that the symmetric and antisymmetric modes have characteristic excitation functions defined by $\alpha_{jq} = 0.5 + G_{jq}/4\pi$ and $\alpha_{jq} = 0.5 - G_{jq}/4\pi$ respectively. The numerical results obtained with the scheme of Fig. 1a agree exactly with this simple model.

The boundary charge method has been successfully employed [18] to assess the importance of edge effects in the loss spectra from aligned MgO cubes with various possible trajectories (e.g. near the middle of a face or near a corner). Figure 2 shows for example a comparison between the experimental STEM and computed loss spectra for a 100 keV electron travelling near and just inside the edge of a cube. The theory successfully reproduces the structure below 15 eV (most of which arises from the most prominent edge mode and had been observed in earlier experiments [22]), but there is a discrepancy of almost a factor of two in the absolute scale. At least part of this may be due to the difficulty of normalizing the experimental spectrum to the zero loss component. The losses observed experimentally below the band gap may be due to defects.

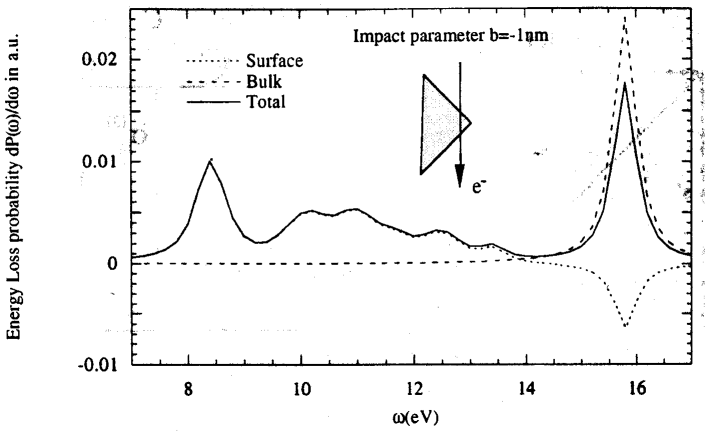

Fig. 2 Energy loss probability for a 100 keV electron impinging on an MgO wedge as shown in the inset. The impact parameter is 1 nm inside the edge. Bulk and surface contributions to the losses are shown [18].

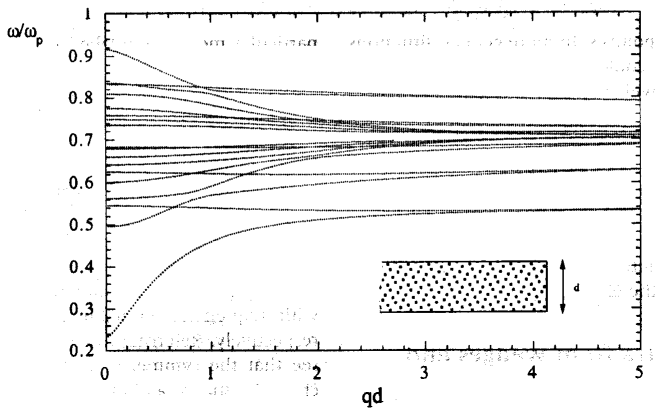

Fig. 3 Spectrum of modes for the truncated end of an Al metallic slab (see inset) as a function of the dimensionless parameter qd [19]. The dielectric function of the slab is characterised by a plasmon frequency ω_p.

An interesting case which has received some attention [6,22,23] is the so-called ALOOF beam configuration when the fast electron beam travels parallel to but a few nm outside a surface such as the face of an MgO cube. Surface, or near surface, valence excitations can be probed in this way without the complicating effects of strong elastic scattering or damaging core excitations which would occur for a penetrating beam [11]. So far the analysis of ALOOF beam spectra has assumed an infinitely extended surface and neglected the contributions from any terminating edges or corners. A preliminary numerical investigation of these effects has been carried out [18,19] for the truncated slab geometry shown in the inset to Fig. 3. In this figure, the behaviour of the various edge modes is shown as a function of qd where d is the slab thickness and q the mode wave vector normal to the diagram. For small values of qd the modes at the top and bottom edges are interactively coupled to form new symmetrical and antisymmetrical combinations with different frequencies. For qd > 2 (or approximately $\omega d/v > 2$) however the two edges can be treated independently and the effect on the loss spectrum can be evaluated fairly simply [18,19].

More complex dielectric junctions

A very important but more complicated 90° wedge situation arises at the junction of three media e.g. at the edge

points where the interface between two media A and B in a thin film cuts the interface with the vacuum. This I junction configuration, depicted in Fig. 1b is (with $\varepsilon_c = 1$) the one most frequently employed in TEM or STEM spectroscopy of interfaces but the effects of the top and bottom surfaces of the film as well as the dielectric wedges formed at the corners is generally ignored. The numerical approach to find the eigenfunctions in a single computation valid for any combination of media then generally fails but has been successfully elaborated [17,19] to deal with such cases. It is interesting to note however that the analysis employed for the isolated wedge in eq. (5) can usefully be extended for this case. Since the dielectric interfaces are now all different, in place of we now use

$$\Lambda_1(\omega) = 2\pi\,(\varepsilon_C + \varepsilon_A)/(\varepsilon_C - \varepsilon_A);\ \Lambda_2(\omega) = 2\pi\,(\varepsilon_C + \varepsilon_B)/(\varepsilon_C - \varepsilon_B);\ \Lambda_3(\omega) = 2\pi\,(\varepsilon_B + \varepsilon_A)/(\varepsilon_B - \varepsilon_A)$$

Using the same notation as before, the eigenmode equations for the T junction region at the top of the film then become

$$\begin{aligned} \Lambda_1(\omega)\sigma_{jq}^{(1)}(s) &= -G_{jq}\,\sigma_{jq}^{(3)}(s) \\ \Lambda_2(\omega)\sigma_{jq}^{(2)}(s) &= -G_{jq}\,\sigma_{jq}^{(3)}(s) \\ \Lambda_3(\omega)\sigma_{jq}^{(3)}(s) &= -G_{jq}\,\sigma_{jq}^{(1)}(s) + G_{jq}\,\sigma_{jq}^{(2)}(s) \end{aligned} \qquad (6)$$

where the purely geometrical integral G_{jq} has exactly the same value as for the isolated 90° wedge. We then find that the mode frequencies are defined by the equation

$$\Lambda_1(\omega)\Lambda_2(\omega)\Lambda_3(\omega) = \{\Lambda_2(\omega) - \Lambda_1(\omega)\}G_{jq}^2 \qquad (7)$$

It then follows that the T junction modes, their excitations and their contributions to the energy loss for a given trajectory can all be related to the properties of the isolated wedge already investigated. The complete case of the I junction shown in Fig. 1b would involve interactive coupling between the two T junctions at top and bottom in the case of a very thin film. Reference to the truncated slab results indicates however that for film thicknesses qd or $\omega d/v > 2$ the two T junctions will be effectively decoupled.

Relativistic effects and radiation

Relativistic corrections both in the form of the mode excitation functions and stopping power contributions A_j in eq. (1) of the above theory become necessary in high voltage electron spectroscopy since even at 100 keV $v/c = 0.55$. Moreover, the Cherenkov process of radiation emission in a dielectric offers an additional channel of energy loss for electrons of velocity $v > c/\varepsilon_1^{1/2}$. Independently of the incident electron energy however the excited modes can decay by the emission of transition radiation as well as by electronic damping and retardation effects can produce significant changes in the form and frequency of modes (particularly low-order modes) with characteristic wavelength $a > c/\omega$. All of these effects are most simply and automatically included in relativistic energy loss theories but only a small number of examples have been worked out. Kroger [24] obtained relativistic analytical solutions for the dielectric losses of an electron passing through a dielectric slab. The case of a relativistic electron moving parallel to a planar dielectric interface was later analysed by Gras Marti *et al.* [25] and successfully compared with experiment by Moreau *et al.* [26] in the case of the Si/SiO_2 interface. An analytical solution for an isolated sphere has also been obtained recently [27]. It is difficult to apply the relativistic theory analytically to other geometries however and it is therefore particularly significant that the boundary charge numerical method can be generalized [28] for the relativistic regime.

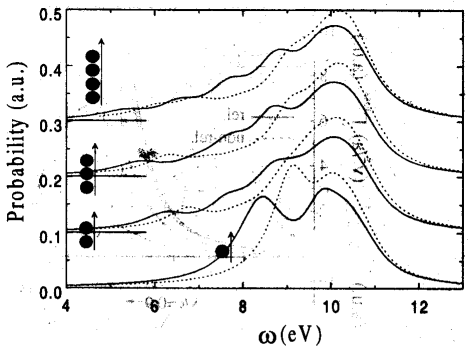

Fig. 4 Loss probability per unit energy range and per sphere for a 100keV electron travelling in vacuum parallel to the axis of symmetry of a set of 1–4 aligned Al spheres and passing at 1 nm from their surfaces [28]. Consecutive curves are relatively shifted upwards by 0.1 a.u for clarity. The spheres have radius 10 nm, separation 1 nm and a free electron dielectric response with $\omega_p = 15.8$ eV and damping $\eta = 1.06$ eV. Solid (broken) curves refer to the relativistic (non-relativistic) computation. The total loss probability is about 2.2% per sphere in all cases.

Although a good deal of the simple physics of the non-relativistic boundary method survives, we now have to deal with boundary charges and currents interacting self-consistently through the electromagnetic field. An extra complication which arises is that the velocity of light (and hence the Green function) is different in the different dielectric regions. Nevertheless, numerical solutions for the eigenmodes, their contributions to the energy loss spectrum as well as the intensity spectrum and angular distribution of any emitted radiation can be computed. Once again the computations are faster for cases where there is an axis along which the dielectric boundaries are either invariant or have axial symmetry. Figure 4 shows a comparison of relativistically and non-relativistically computed loss spectra for one, two, three and four Al spheres interacting along a line parallel to the incident beam. The relativistic shift of the modes is readily apparent as well as the effects of the inter-sphere coupling in the low energy range. The dependence of the loss spectrum from a single Al sphere on electron velocity and sphere

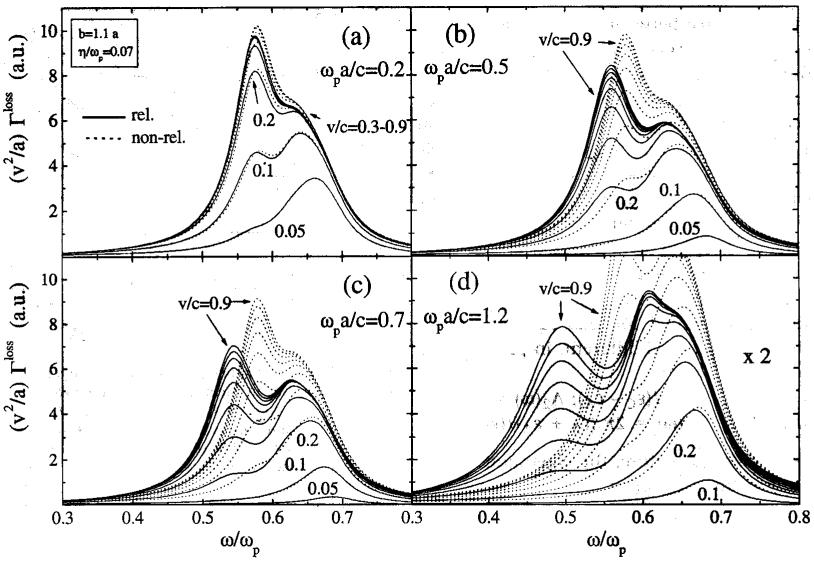

Fig. 5 Scaled loss probability (a single sphere) as a function of fast electron velocity v and sphere radius a [27]. The sphere is characterized by a free electron dielectric response with ω_p = 15.8 eV and damping parameter $\eta = 0.07\omega_p$. The impact parameter (measured from the sphere centre) is 1.1a.

size is shown in Fig. 5 with the non-relativistic results again included for comparison. The electron passes just outside the sphere. The contributions due to the l = 1 (dipole), l = 2 and l = 3 modes can be seen. Their amplitudes, but not their positions, depend on the electron velocity. The mode positions are strongly affected by retardation effects, particularly for the larger spheres and lower l values. For instance the dipole mode of the largest sphere (in Fig. 5d) appears below 0.5 ω_p instead of at $\omega_p/3^{1/2}$ as in the non-relativistic theory. The probability of radiative decay (emission of transition radiation) is greatest for the dipole mode and falls off with increasing l. Figure 6 shows how the total loss probability is divided between electronic damping and radiation emission for the different modes as a function of the electronic damping.

It appears that the transition radiation emission probability from typical nanostructures per incident fast electron may approach 0.5% and be sufficiently intense to provide a useful additional source of spectral information about local electronic and geometrical structure. In recent TEM experiments [29], transition radiation and Cherenkov radiation have both been detected from thin films and can readily be computed by the relativistic boundary method. Transition radiation from the dipole l = 1 and quadrupole l = 2 modes of Ag spheres and the dependence of the emission wavelength on sphere size has also recently been noted (N. Yamamoto – private communication). These results may possibly be explained by the retardation effect. In other cases however, such as the size-dependence

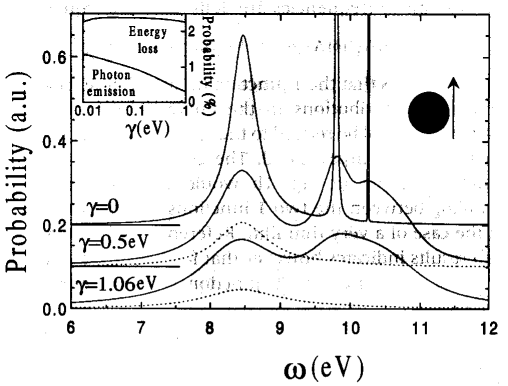

Fig. 6 Loss probability (solid curves) and photon emission probability (broken curves) for a 100 keV electron passing at 1nm from a 10 nm radius sphere described by a free electron response function with ω_p = 15.8 eV and various levels of electronic damping shown. The inset shows the total probability as a function of damping [28].

of the bulk mode observed in small Si particles [30], the explanation depends on quantum size effects as well as the spill-over of the valence charge density beyond the geometrical boundary [31]. Both of these phenomena signal a failure at these small volumes of the local macroscopic dielectric function used here to characterize each dielectric region.

Conclusions

The boundary charge method offers a convenient means of computing spatially localized valence loss spectra from arbitrary structures in the non-relativistic regime. When only two media are involved in a geometry which is invariant along one axis or has axial symmetry, the computations are particularly fast and the geometry is cleanly separated from the dielectric response of the components. Important cases, such as a planar interface between two media in a thin film studied in HREM profile imaging, can now be solved exactly in terms of simpler structures.

At some increase in complexity, the boundary method has been developed for relativistic situations when either fast electrons are involved or when it is desired to compute the radiation emitted from a complex structure.

Since a very large variety of problems can now be tackled by these methods, priority should be given to situations where experimental data are already available or likely to be available. Apart from the planar interface case just noted, the cases of small particles of well-defined shape (such as MgO smoke cubes) or nanotubes deserve attention.

The combination of spatially resolved valence EELS and optical emission spectroscopy appears both practical and interesting. To distinguish experimentally between transition radiation, Cherenkov radiation and other forms of cathodoluminescence it might be useful to employ coincidence detection methods like those already used for valence losses and secondary electron emission.

Spectroscopy of emitted photons is a potentially a useful technique in the context of the STM. The radiation spectrum is however a sensitive function of the local tip-sample geometry as well as of the dielectric response of the materials concerned. The relativistic boundary method should be useful in computing these effects. It is also in principle capable of computing van der Waals interactions in arbitrary geometries.

References

1 Echenique P M and Pendry J B (1978) Absorption profile at surfaces. *J. Phys. C* **8**: 2936–2942.

2 Howie A and Milne R H (1985) Excitations at interfaces and small particles. *Ultramicroscopy* **18**: 427–434.

3 Bleloch A L, Howie A, Milne R H, and Walls M G (1989) Elastic and inelastic scattering effects in reflection electron microscopy. *Ultramicroscopy* **29**: 175–182.

4 Walsh C A (1989) Analysis of electron energy loss spectra from electron-beam-damaged amorphous Al_2O_3. *Philos. Mag. A* **59**: 227–246.

5 Zabala N, Rivacoba A, and Echenique P M (1989) Energy loss of electrons travelling through cylindrical holes. *Surface Sci.* **209**: 465–480.

6 Batson P E (1982) Surface plasmon coupling in clusters of small spheres. *Phys. Rev. Lett.* **49**: 936–940.

7 Ferrell T L and Echenique P M (1985) Generation of surface excitations on dielectric spheres by an external electron beam. *Phys. Rev. Lett.* **55**: 1526–1529.

8 Echenique P M, Howie A, and Wheatley D J (1987) Excitation of dielectric spheres by external electron beams. *Philos. Mag. B* **56**: 335–348.

9 Ugarte D, Colliex C, and Trebbia P (1992) Surface and interface plasmon modes on small semiconducting spheres. *Phys. Rev. B* **45**: 4332–4343.

10 Zabala N, Rivacoba A, and Echenique P M (1997) Coupling effects in the excitations by an external electron beam near close particles. *Phys. Rev. B* **56**: 7623–7635.

11 Walls M G and Howie A (1989) Dielectric theory of localised valence electron spectroscopy. *Ultramicroscopy* **28**: 40–42.

12 Howie A and Walsh C A (1991) Interpretation of valence loss spectra from composite materials. *Micrcrosc., Microanal. & Microstruct.* **2**: 171–181.

13 Barrera R and Fuchs R (1995) Theory of electron energy loss in a random system of spheres. *Phys. Rev. B* **52**: 3256–3273.

14 Fuchs R (1975) Theory of the optical properties of ionic crystal cubes. *Phys. Rev. B* **11**: 732–740.

15 Ouyang F and Isaacson M (1989) Surface plasmon excitation of objects of arbitrary shape and dielectric constant. *Philos. Mag. B* **60**: 481–492.

16 Ouyang F and Isaacson M (1989) Accurate modelling of particle-substrate coupling of surface plasmon excitations in EELS. *Ultramicroscopy* **31**: 345–350.

17 Garcia de Abajo F J and Aizpurua J (1997) Numerical simulation of electron energy loss near inhomogeneous dielectrics. *Phys. Rev. B* **56**: 15873–15884.

18 Aizpurua J, Rafferty B, Garcia de Abajo F J, and Howie A (1997) Numerical simulation of valence losses in MgO cubes. In: *Electron Microscopy and Microanalysis 1997*, ed. Rodenburg J, pp. 277–280, (Inst. of Physics, Bristol).

19 Aizpurua J, Garcia de Abajo F J, and Howie A (1999) Valence electron energy loss near edges, truncated slabs and junctions. *Phys. Rev. B* **60**: 11149–11162.

20 Dobrzynski L and Maradudin A A (1972) Electrostatic edge modes in a dielectric wedge. *Phys. Rev. B* **6**: 3810–3815.

21 Davis L C (1976) Electrostatic edge modes of a dielectric wedge. *Phys. Rev. B* **14**: 5523–5525.

22 Marks L D (1982) The image force for fast electrons near an MgO surface. *Solid State Comm.* **43**: 727–729.

23 Mullejans H, Bleloch A L, Howie A, and Tomita M (1993) *Ultramicroscopy* **52**: 360–368.

24 Kroger E (1970) Transition radiation, cerenkov radiation and energy loss of relativistic charged particles traversing thin foils at oblique incidence. *Z. Phys.* **235**: 403–421.

25 Garcia Molina R, Gras Marti A, Howie A, and Ritchie R H (1985) *J. Phys.* **18**: 5335–5345.

26 Moreau P, Brun N, Walsh C A, Colliex C, and Howie A (1997) Relativistic effects in electron-energy-loss-spectroscopy observations of the Si/SiO_2 interface plasmon peak. *Phys. Rev. B* **56**: 6774–6781.

27 Garcia de Abajo F J (1999) Relativistic energy loss and induced photon emission in the interaction of a dielectric sphere with an external electron beam. *Phys. Rev. B* **59**: 3095–3107.

28 Garcia de Abajo F J and Howie A (1998) Relativistic electron energy loss and electron-induced photon-emission in inhomogeneous dielectrics. *Phys. Rev. Letts.* **80**: 5180–5183.

29 Yamamoto N, Sugiyama H, and Toda A (1996) Cherenkov and transition radiation from thin plate crystals detected in the transmission electron microscope. *Proc. R. Soc. A* **452**: 2279–2301.

30 Mitome M, Yamazaki Y, Takagi H, and Nakagiri T (1992) Size-dependence of plasmon energy in Si clusters. *J. Appl. Phys.* **72**: 812–814.

31 Eckardt W (1985) Size dependent photoabsorption and photoemission of small metal particles. *Phys. Rev. B* **31**: 6360–6370.